Tuning the magnetic properties of oleic-acid-coated cobalt ferrite nanoparticles by varying the surfactant coverage

*Marianna Vasilakaki, Nikolaos Ntallis, Kalliopi N. Trohidou**

Institute of Nanoscience and Nanotechnology, NCSR "Demokritos", 153 10 Agia Paraskevi, Attiki, Greece

Keywords: coating materials, spinel ferrite nanoparticles, anisotropy, magnetization, Monte Carlo simulations, DFT calculations

ABSTRACT

Organic coatings on magnetic nanoparticles are extensively used in various applications. As demonstrated recently, these coatings affect the magnetic behavior of the nanoparticles. The modification of the magnetic properties of the nanoparticles and nanoparticle assemblies, as the percentage of the oleic acid (OA) coverage of a cobalt ferrite nanoparticle increases, is investigated numerically using a multiscale modeling approach that combines density functional theory (DFT) and Monte Carlo simulations. The DFT calculations show that the increase in OA coverage results in a monotonic decrease of the mean magneto-crystalline anisotropy and in a reduction of the atomic magnetic moments and the exchange coupling constants in the nanoparticle. These effects are attributed to the gradual recovery of the bulk spinel structure at the coated surface, as the OA

coverage increases. Input from the DFT calculations is used in the mesoscopic modeling for the study of the magnetic behavior of an assembly of these nanoparticles by employing the Monte Carlo simulations technique. The results demonstrate that despite the decrease of magnetic anisotropy, the coercive field increases with the increase in percentage of OA coverage in the assembly, in agreement with experimental findings. This study suggests the possibility of tailoring the magnetic properties of cobalt ferrite nanoparticles for high-performance applications by varying the organic coating concentration.

1. Introduction

In recent decades, magnetic nanoparticles (MNPs) have greatly contributed to the development of a variety of cutting-edge technologies in fields such as biomedicine [1–3], environment [4,5] and energy [6], in the form of solid nanostructures and ferrofluids [7,8]. In these applications, nanoparticles exist in assemblies and tend to aggregate, often deteriorating the magnetic properties of the system [9]. To prevent this major drawback, one solution is coverage of the surface of these MNPs with an organic coating during or after their preparation.

The choice of organic coating is of great importance since it affects single and consequently collective magnetic properties of the nanoparticles. Indeed, the presence of a surfactant is often associated with different surface ion distribution [10] or surface spin arrangement, leading to the increase [11] or decrease of surface disorder [12–14]. This also influences the local effective magnetic anisotropy [15,16], the exchange coupling forces between the surface spins [10] and the particle saturation magnetization [10,17,18]. As a result, different ligands bonded at the surface of the MNPs affect the coercive field [19,20], the blocking temperature [21] and their magneto-hydro-dynamic response [22]. In some cases, clustering of MNPs occurs during the coating process,

resulting in additional magnetic effects in an assembly [23–25]. The coating affects both the intraparticle characteristics and the interparticle interactions, offering the possibility of controlling the nanoparticles' magnetic behavior. The choice of an appropriate coating is essential for applications, particularly those requiring good colloidal stability of MNPs in liquids [26] and particles' biocompatibility [27,28].

The growing interest in coated MNPs, mainly iron-oxide based nanoparticles [21,25,29–36], focuses mainly on the fundamental understanding of the effect of the surfactant molecules on their magnetic properties. Less attention has been given to the effect of the amount of surface coverage, which is related to the particle synthesis protocol by which different MNP parameters (e.g. shape and size) are changed simultaneously. Although electronic structure calculations have been performed on uncoated spinel ferrite nanoparticles [25,37–39] in recent years, very few electronic structure calculations are reported on nanoparticles covered with organic ligands (see [40,41] on small Co clusters coated with varying percentage of organic or C–O molecules attached at their surface). These studies demonstrated that the different percentage of these molecules can affect their magnetic behavior. Furthermore, the effect of the coating depends on its type and on the MNP type (size and structure). The study of magnetic behavior becomes more complicated when ferrite nanoparticles are involved, because the bonding between metal atoms is replaced by the complex bonding between the transition metal (TM) ion and the O ion.

Cobalt ferrite ($CoFe_2O_4$) nanoparticles are among the most promising materials for biomedical (hyperthermia and magnetic particle imaging), environmental and technological applications [2,4,6,42–46] because of their high magneto-crystalline anisotropy. An oleic acid (OA, $C_{17}H_{33}COOH$) coating is commonly used for the preparation of $CoFe_2O_4$ nanoparticles, which provides steric stabilization against van der Waals and magnetic dipolar forces and thereby

prevents agglomerations; it also reduces the toxic effects of these nanoparticles [47,48]. Experimental results on the effect of the OA coating concentration on the magnetic behavior of the $CoFe_2O_4$ nanoparticles by Limaye et al. [51] showed that as the concentration of OA increases, the coercivity also increases. However, Jovanovitch et al. [50] found that the OA covalently bonded to the $CoFe_2O_4$ nanoparticle surface decreases the surface anisotropy and the coercive field of the ~6-nm OA-coated nanoparticles with the increase in OA surface coverage.

In this work, we investigate the effect of the OA surface coating concentration on the magnetic behavior of $CoFe_2O_4$ nanoparticle assemblies to elucidate the intriguing role of the increase of the number of OA molecules on the magnetic properties of the $CoFe_2O_4$ nanoparticles when bonded on their surface. Previous atomic- and mesoscopic-scale studies on the magnetic behavior of uncoated spinel ferrite nanoparticles introduced in the spin Hamiltonian the relevant intraparticle exchange coupling constants extracted from density functional theory (DFT) calculations on the corresponding bulk materials or from experimental considerations [24,52–54]. Here we take a step forward, by extracting the intraparticle magnetic parameters from DFT calculations, explicitly performed on OA-coated $CoFe_2O_4$ nanoparticles, taking into account the spinel structure and the core/surface morphology at the atomic (single particle) and the mesoscopic scale (assembly) [10]. We propose a multiscale modeling approach at three length scales: (1) DFT calculations on an OA-capped spherical $CoFe_2O_4$ particle of ~2 nm size with varying OA surface coverage, (2) atomic-scale calculations using input from the DFT results, for a spherical core/surface nanoparticle with the inverse spinel ferrite structure of 5 nm size (as in the experimental situation of [10,50]) with modified surface properties due to the OA coating and (3) a mesoscopic-scale approach for assemblies of core/surface nanoparticles of 5 nm size each, by rescaling the atomic-scale parameters and including interparticle interactions. Our systematic study provides a thorough

understanding of the underlying mechanism of the coating–nanoparticle interaction along the organic–inorganic interface and its effect on the macroscopic behavior of the assemblies. Thus, we can achieve better control of the magnetic properties of the $CoFe_2O_4$ nanoparticles covered with OA.

2. Theoretical calculations

Multiscale modeling is employed to investigate the hysteresis behavior of $CoFe_2O_4$ nanoparticles in the presence of OA coating by varying the percentage of surface coverage.

2.1 Electronic structure calculation of MNP parameters

The DFT calculations are performed based on spin-polarized DFT [55,56], implemented by the Vienna Ab Initio Simulation Package (VASP) code, in an inverse spinel ferrite nanoparticle with stoichiometric chemical formula $CoFe_2O_4$.

In our calculations the electronic charge density and the local potential are expressed in plane wave basis sets. The exchange correlation functional chosen is the one proposed by Perdew–Burke–Ernzerhof. The interactions between the electrons and ions are described using the projector augmented wave method and the GGA + U approach to treat localized states as proposed by Dudarev et al. [57]. All studied geometries are fully optimized (electronic relaxation, 10^{-4} eV; ionic relaxation, 10^{-3} eV). The initial structures are formed by replication of the bulk unit cell followed by a trimming procedure in order to obtain the spherical shape for the nanoparticles. The resulting structure is a spherical nanoparticle with inverse spinel structure and diameter $D \sim 2$ nm containing 246 atoms (70 Fe, 36 Co and 140 O atoms). Moreover, an empty space of 1.5 nm is used in all directions in order to avoid interaction with periodic images. For this $CoFe_2O_4$ nanoparticle, different numbers of bonded organic acid molecules (each containing 18 C, 2 O and

34 H atoms) per nanoparticle's surface area, are considered for the different percentages of the surface coverage. The spins of the TM ions between the A-sites and between the B-sites are ordered ferromagnetically and antiferromagnetically between the A–B sites in the initial spin configuration [59]. **Fig. 1** shows the most stable energy configuration (where the carboxylic acid coordinates with the metal ions as a monodentate ligand) found after several simulated structural relaxations, starting from different initial configurations.

We calculate the magnetic moments, the magneto-crystalline anisotropy energy (MAE) and the exchange coupling constants for the $CoFe_2O_4$ nanoparticle covered with 2, 3, 4, 6, 8, 11, 16, 19 and 22 OA molecules corresponding to 2.5%, 3.75%, 5%, 7.5%, 10%, 14%, 20%, 24% and 27% percentage of surface coverage, respectively. In **Fig. 1**, the relaxed structures for 5% and 7.5% surface coverage are shown.

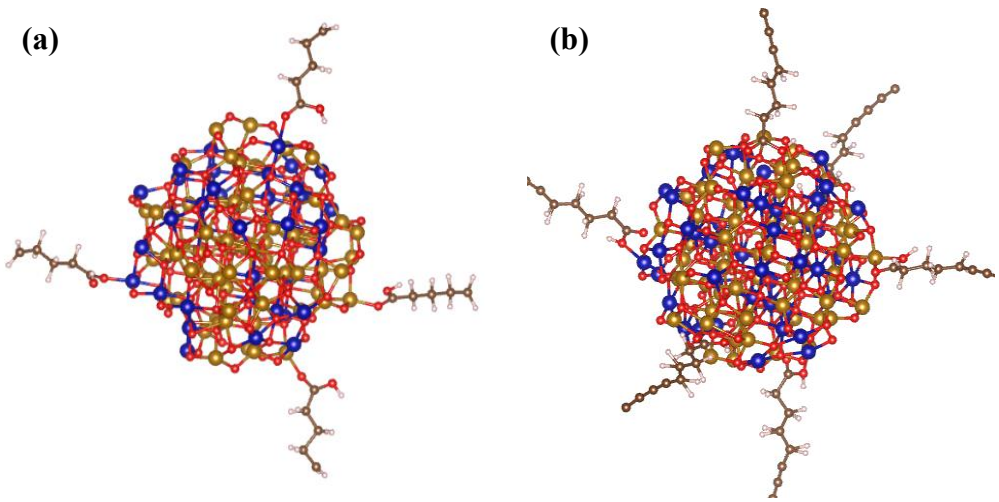

Fig. 1. Relaxed structures of $CoFe_2O_4$ spherical nanoparticles with increasing number of organic molecules attached on their surface, corresponding to OA coverage of 5% (a) and 7.5% (b) (Fe (yellow), Co (bleu), O (red), C(brown), H(white)). For simplicity, OA molecules are not fully shown.

In **Table 1**, we calculate the total mean magnetic moment of the nanoparticle and the mean magnetic moment for each of the metal ions as a function of the OA surface coverage. In the calculation, the induced magnetic moment of the O atoms is also included. The total mean magnetic moment decreases as OA coverage increases. The decrease is faster with the increase of coverage up to 10% and then much slower up to 27%. The same decreasing trend is also observed for the mean magnetic moments of Fe^{3+}_{A} and Co^{2+}_{B}, with the Co moments to decrease faster than those of the tetrahedral Fe ions, with the increase of surface coverage. The effect of the OA coverage on the mean magnetic moments of the octahedral Fe ions is slightly different. The rate of decrease is slower than the other metal ions and it increases above 20%. In addition, the MAE in the ground state of the system is calculated for several spin orientations, including spin–orbit coupling, by rotating all spins coherently along different directions. In **Table 1**, we show the change in the magnetic anisotropy energy (MAE) with the increase of OA molecules. We observe that MAE decreases slowly with the increase of OA surface coverage.

Table 1 DFT calculations of the total mean magnetic moment and for each metal ion and the corresponding magnetic anisotropy energy (MAE) with the increase of OA molecules coating.

Oleic Acid coverage (%)	Mean Moment(μ_B)	Fe^{3+}_{A} (μ_B/atom)	Fe^{3+}_{B} (μ_B/atom)	Co^{2+}_{B} (μ_B/atom)	MAE (meV)
0.00	125.8	4.190	4.250	2.780	11.50
2.50	124.4	4.150	4.200	2.750	11.40
3.75	123.2	4.090	4.120	2.710	11.30
5.00	122.4	4.010	4.080	2.660	11.20
7.50	122.5	3.800	4.050	2.400	11.10
10.00	121.4	3.599	3.909	2.241	10.90
14.00	120.8	3.587	3.890	2.230	10.86
20.00	120.4	3.579	3.890	2.231	10.80
24.00	120.1	3.578	3.789	2.231	10.72
27.00	119.5	3.570	3.570	2.212	10.70

In order to calculate the magnetic exchange coupling constants, different magnetic configurations are mapped on a Heisenberg model with first-neighbor interactions. The mapped magnetic configurations are created by randomly flipping the magnetic moments of both sublattices starting from the ground state configuration of the system [10]. In this way we determine the mean exchange coupling constants between A–A, B–B and A–B ions for the uncoated nanoparticles (J_{AA} = 13.759 meV, J_{BB} = 16.758 meV and J_{AB} = −22.62 meV, respectively) and for the OA-coated nanoparticles (J_{AA} = 10.72 meV, J_{BB} = 12.96 meV and J_{AB} = −17.28 meV, respectively).

There is a decrease in the exchange coupling constants of the coated nanoparticles that can be attributed to the variation of the surface structure. Comparing these exchange coupling constants with their bulk values [60] shows a gradual decrease of the exchange coupling strength between B–B octahedral ions and between A–B sites, because of the surface modifications (lattice distortions and coordination number).

In the uncoated nanoparticle, the symmetry breaking at the surface of the $CoFe_2O_4$ nanoparticles due to the absence of some oxygen atoms results in the increase of the spin–orbit coupling, which is responsible for enhanced magneto-crystalline surface anisotropy [61,62]. The OA can be considered as effectively taking the position of these missing atoms. Indeed, as the metal cations at the surface of nanoparticles are coordinated with OA, the spin−orbit coupling and the magnetic moment become smaller as previously demonstrated [62]. The reduced spin–orbit coupling also leads to the decrease of the surface anisotropy affecting MAE (see **Table 1**).

The results of our DFT calculations for the magnetic moments, the exchange coupling constants and the anisotropies are used as input data in the atomic-scale modeling for the hysteresis

behavior of a nanoparticle and in the mesoscopic-scale modeling of the corresponding nanoparticle assemblies.

2.2 Atomic-scale simulations of a $CoFe_2O_4$ nanoparticle

The nanoparticle size of D = 2 nm in our DFT calculations is the maximum size, we could achieve, because of the computational cost (time and size) of these electronic structure calculations. Next, we model a spherical $CoFe_2O_4$ nanoparticle of 5 nm size and cubic inverse spinel structure with lattice constant 0.835 nm (as found in our DFT calculations). The 5 nm particle size is selected for comparison with previous experimental findings [10]. In **Fig. 2**, the model of the $CoFe_2O_4$ nanoparticle of cubic inverse spinel is shown. All the magnetic atoms are placed at the lattice sites and they are represented by classical spins $\mathbf{s}_i$ with $|\mathbf{s}_i| = 1$. Oxygen atoms are not shown in **Fig. 2**, however, their magnetic moments, though almost negligible, they have been already incorporated into our calculations. We consider a core/surface structure with a disordered surface layer of thickness equal to one lattice constant [63,64].

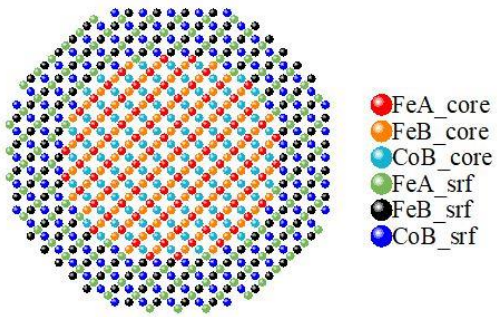

Fig. 2. Two-dimensional schematic representation of the simulated model of $CoFe_2O_4$ spherical nanoparticle of 5 nm size. The metal ions in the core and at the surface are shown.

The energy of the system (Eq. 1) includes the Heisenberg exchange interaction term between nearest neighbors in the core and at the surface (first and second term, respectively), the Zeeman energy (third term) and the anisotropy energy of the core (with cubic magneto-crystalline

anisotropy) and at the surface (uniaxial with random orientation of the easy axis at each site i given by the random unit vector $\hat{\mathbf{e}}_i$) (fourth and fifth term, respectively).

$$\mathcal{E} = -\sum_{<i,j\in core>}^{N} J_c \vec{s}_i \cdot \vec{s}_j - \sum_{<i,j\in srf>}^{N} J_{srf} \vec{s}_i \cdot \vec{s}_j - \mu_0 \vec{H} \cdot \sum_{i=1}^{N} \vec{s}_i$$
$$- \sum_{i\in core}^{N} K_{i\_core} \left(s_{x,i}^2 \cdot s_{y,i}^2 + s_{y,i}^2 \cdot s_{z,i}^2 + s_{z,i}^2 \cdot s_{x,i}^2 \right) - \sum_{i\in srf}^{N} K_{i\_srf} \left(\vec{s}_i \cdot \hat{e}_i \right)^2 \quad (1)$$

In equation (1) the core exchange coupling constant J_C is calculated from the bulk J_{AA}, J_{BB} and J_{AB} of the A–A, B–B and A–B interactions [60], respectively. For the calculation of the core anisotropy constants for the Fe (K_{Fe_core}) and Co atoms (K_{Co_core}), we start from the bulk value for the cubic magnetocrystalline anisotropy of $CoFe_2O_4$, $K = 20 \times 10^4$ J m^{-3} [65] . The core of the particle contains 24 metal ions, therefore the calculation of the bulk anisotropy of the core gives K_{core} = 0.2976 meV. From there, we get K_{Co_core}=0.031 and K_{Fe_core} =0.0031, taking into account that K_{Co_core}= 10 × K_{Fe_core} [65].

For the surface parameters, the corresponding exchange coupling and anisotropy constants are taken from the DFT calculations, performed on the 2-nm particle, since for this nanoparticle size more than 90% of the magnetic atoms belong to the surface. As we showed in the Section 2.1, for coverage above 10%, the MAE and the total mean magnetic moment very little vary with the increase of the OA coverage. Therefore, for the surface anisotropy constants of the Fe (K_{Fe_srf}) and Co atoms (K_{Co_srf}), we use the anisotropy constants extracted from the DFT calculation of MAE for a $CoFe_2O_4$ particle with 106 metal ions. We calculate the corresponding K_{Fe_srf} and K_{Co_srf} values for all OA coverage cases, using the relation $K_{srf} = 70\times K_{Fe\_srf} + 36\times K_{Co\_srf} = 70\times K_{Fe\_srf} + 36\times 10\times K_{Fe\_srf} = 430 \times K_{Fe\_srf}$. Along these lines, the anisotropy constants for the different OA

concentrations are listed in **Table 2**. All the energy terms in Eq. 1 are divided by the exchange coupling of a perfect antiferromagnet J_{AFM} = 1.0 meV to be dimensionless.

Table 2. The anisotropy constants for the surface metal atoms.

OA surface coverage (%)	K_{Fe}	K_{Co}
0	0.0267	0.267
5	0.0260	0.260
10	0.0253	0.253
20	0.0251	0.251
27	0.0249	0.249
100	0.0230	0.230

2.3 Mesoscopic-scale simulations of an assembly of $CoFe_2O_4$ nanoparticles

In our previous studies [10,23–25,66–68], we developed a mesoscopic model to study the magnetic behavior of assemblies of nanoparticles with core/surface morphology. This model describes each nanoparticle with a classical spin ($\mathbf{s}_{1i}$) for the core and two spins ($\mathbf{s}_{2i}$, $\mathbf{s}_{3i}$) for the two surface sublattices as previously described [10]. We consider magnetic interparticle interactions between the nanoparticles in the assembly. Our model is based on the reduction of the number of the simulated spins to the minimum adequate to describe the core/surface morphology for each nanoparticle. The effect induced by OA molecules bonded on the nanoparticle surface is included in the magnetic moment and the anisotropy values. We use this model to simulate an assembly of $CoFe_2O_4$ nanoparticles each of diameter D = 5 nm. In the case of the uncoated particles, we consider a dense assembly of 50% particle concentration and a particle concentration of 20% for the OA-coated nanoparticle assemblies because the particles are dispersed in larger distances due to the presence of the OA molecules on their surface. The particles are randomly located on the

nodes of a simple cubic lattice in a box of dimensions $10\alpha \times 10\alpha \times 10\alpha$, where α is the smallest interparticle distance and is equal to particle diameter, in order to avoid particles overlapping. The energy of the system is given by the following expression [69]:

$$\mathcal{E} = -\sum_{i=1}^{N}\left\{k_C\left(\hat{s}_{1,i}\cdot\hat{e}_{1,i}\right)^2 + k_{srf}/2\left[\left(\hat{s}_{2,i}\cdot\hat{e}_{2,i}\right)^2+\left(\hat{s}_{3,i}\cdot\hat{e}_{3,i}\right)^2\right]\right\}$$
$$-\sum_{i=1}^{N}\left[j_{c1}\left(\hat{s}_{1,i}\cdot\hat{s}_{2,i}\right)+j_{c2}\left(\hat{s}_{1,i}\cdot\hat{s}_{3,i}\right)+j_{surf}\left(\hat{s}_{2,i}\cdot\hat{s}_{3,i}\right)\right]$$
$$-g\sum_{\substack{i,j=1\\ i\neq j}}^{N}\left(m_{1,i}\hat{s}_{1,i}+m_{2,i}\hat{s}_{2,i}+m_{3,i}\hat{s}_{3,i}\right)D_{ij}\left(m_{1,j}\hat{s}_{1,j}+m_{2,j}\hat{s}_{2,j}+m_{3,j}\hat{s}_{3,j}\right)$$
$$-\sum_{<i,j>}^{N}\left[j_{ex}\left(\hat{s}_{2,i}\cdot\hat{s}_{2,j}\right)+j_{ex}\left(\hat{s}_{3,i}\cdot\hat{s}_{3,j}\right)\right]-\mu_0 h\sum_{i=1}^{N}\left(m_{1,i}\hat{s}_{1,i}+m_{2,i}\hat{s}_{2,i}+m_{3,i}\hat{s}_{3,i}\right)\cdot\hat{e}_h \qquad (2)$$

Each spin within a nanoparticle has a uniaxial easy anisotropy axis with a random orientation (first term) and interacts via Heisenberg exchange interaction with the other two spins inside the particle (second term). Thus, the short-range intraparticle exchange interactions between the core spin and each of the two surface spins (interface coupling j_{c1} and j_{c2}) and between the two surface spins (surface coupling j_{srf}) are introduced in our energy calculations together with interparticle dipolar interactions (third term) and interparticle exchange interactions (j_{ex}) between the nanoparticles in contact (fourth term). The last term gives the Zeemann energy. We calculate the normalized magnetic moments $m_1 = M_{core}V_1/M_sV$, $m_2 = M_{srfA}V_2/M_sV$ and $m_3 = M_{srfB}V_3/M_sV$. Here M_s and V are the saturation magnetization and the volume of each particle, and M_{core}, M_{surfA} and M_{surfB} and V_1, V_2 and V_3 are the particle magnetizations and volumes of the core spins and the two sublattices of the surface spins, respectively, calculated from the atomic-scale model. In particular, the atomic scale model gives that the total number of spins is 2680 (514 Fe spins and 268 Co spins in the core and 618 Fe_A spins, 660 Fe_B spins and 620 Co_B spins at the surface) for a 5 nm Co ferrite nanoparticle and the volume ratios are: V_{core}/V_{tot}=0.3, $V_{A\ surf}/V_{tot}$= 0.2, $V_{B\ surf}/V_{tot}$ = 0.5. In **Table 3**, the calculated magnetizations for the two surface sublattices normalized to the total magnetic moment M_{tot} (for OA% = 0) are given. The core magnetization is calculated as M_{core}/M_{tot} = 0.276.

The D_{ij} is the dipolar tensor and $g = \mu_0(M_sV)^2/(4\pi d^3 K_C V_1)$ is the reduced dipolar strength, we set $g = 0.30$.

Table 3. The calculated magnetizations normalized to M_{tot} (for OA% = 0) of the mesoscopic model for the surface for the different percentage of OA coverage.

OA surface coverage (%)	M_{surfA}/M_{tot}	M_{surfB}/M_{tot}
0	0.969	1.694
5	0.927	1.624
10	0.832	1.485
20	0.828	1.478
27	0.825	1.394
100	0.825	1.394

The anisotropy constants inside the different spin regions of the nanoparticle in the mesoscopic-scale model are calculated from our atomic scaling results, by properly rescaling them, to account for the size of the core and surface regions separately. In more detail, DFT calculations of MAE correspond to the volume of a nanoparticle of diameter of 2 nm, so for the surface volume of 5 nm particle, we take $K_{srf}V_{srf}$ = 11× MAE, since V_{srf} (D=5nm) / V_{core} (d=2 nm) = 11. The volume of the core size D_{core}=3.33 nm (D=5 nm) is 33 times larger than the core of the particle of d=2 nm with corresponding K_{core} = 0.2976 meV, thus the core volume anisotropy is $K_{core}V_{core}$=33×0.2976 meV = 10.02 meV. The calculated anisotropy constants for the surface volume anisotropy are 126.5, 123.2, 119.2, 118.8, 117.7 and 93.5 for 0%, 5%, 10%, 20%, 27% and 100% respectively. These constants are normalized to the core volume anisotropy K_CV_1 so they are dimensionless [10], thus the core spin is k_c = 1.0. The anisotropy for each of the two surface spins is k_{srf} /2 and for the different OA surface coverage are shown in **Table 4**. The 100% surface coverage corresponds to a complete layer of OA of 2-nm thickness . The reduced intraparticle exchange coupling constants are calculated from the atomic-scale constants. The interparticle exchange coupling constant j_{ex} is taken as a free parameter and it reduces as the OA surface coverage increases, taking the values 7.8, 6.0, 3.0, 1.5, 0.75 and 0.0 for OA coverage of 0%, 5%, 10%, 20%, 27% and 100%, respectively. In **Table 4** the calculated mesoscopic parameters are summarized. The normalized external magnetic field is denoted by h and the normalized temperature by t.

Table 4. Calculated magnetic moments for the core (m_1) and the surface (m_2, m_3), the anisotropy constants of the core (k_c) and the surface (k_{srf}) and the exchange coupling constants (j_{ex}) for particles in contact of the mesoscopic model for different percentage of OA coverage.

Oleic Acid coverage (%)	m_1	m_2	m_3	k_c	k_{srf}	j_{ex}
0	0.083	0.194	0.847	1	12.63	7.8
5	0.083	0.185	0.812	1	12.30	6.0
10	0.083	0.166	0.742	1	11.97	3.0
20	0.083	0.166	0.739	1	11.86	1.5
27	0.083	0.165	0.697	1	11.75	0.75
100	0.083	0.165	0.697	1	10.85	0.75

The Monte Carlo simulation technique with the implementation of the Metropolis algorithm is used to calculate the low-temperature hysteresis loops for single MNPs and their assemblies after a field cooling procedure. For the dipolar energy calculation in the assembly, the Ewald summation technique [69] is implemented. The Monte Carlo simulation results for a given temperature and an applied field were averaged over 20 samples with various spin configurations, realization of the easy-axes distribution and different spatial configurations for the nanoparticles. For every field value, the first 5×10^2 steps per spin for the assemblies and 10^3 steps per spin for the single nanoparticle are used for equilibration, and the subsequent 7×10^3 and 10^4 Monte Carlo steps per spin in the assemblies and the single nanoparticle respectively are used to obtain thermal averages.

3. Results and discussion

To shed light on the effect of OA coating on the lattice structure of the nanoparticle, we focus first on the DFT results. We compare the calculated radial distribution function (rdf) of the metal

ion-oxygen bond, on the surface of the particle for the uncoated (0% OA) and for the 10% and 20% OA surface coverage case (**Fig. 3**). In the presence of OA, the distribution of the TM–O bond lengths, increases on average, indicating an expansion of oxygen coordination of the TM ions and results in the reduction of magnetization. DFT calculations also show that with the increase of the coordination of the OA-bonded Co and Fe surface ions, the lattice distortion of the Co and Fe ions positions at the nanoparticle's surface gradually reduces. Consequently, the anisotropy and the magnetization decrease as the OA coverage of the particle surface increases. This is also reflected in the change of the exchange coupling strength.

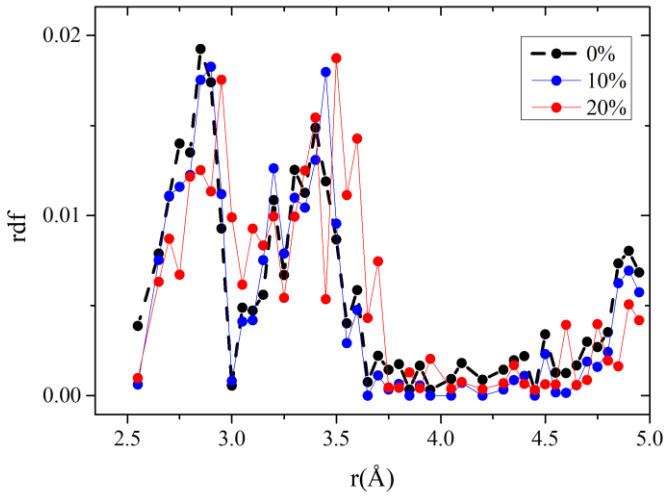

Fig. 3. Radial distribution function (rdf) of the TM–O pairs at the surface of the particle for uncoated (black line) and 10% (bleu) and 20% (red line) OA-coated nanoparticles. The rdf is calculated with a bin size of 0.05 Å .

Next we examine the effect of OA surface coverage on the magnetic behavior of a nanoparticle of size 5 nm, to compare with recent experiments [10], and for nanoparticles in an assembly, where interparticle interactions are present. We use Monte Carlo simulations with the implementation of the Metropolis algorithm [71] to calculate the hysteresis loop at low temperature. The 100%

surface coverage corresponds to the formation of a complete OA monolayer of 2 nm thickness. In **Fig. 4** we show the evolution of the coercive field as the OA surface coverage increases for uncoated and for six different OA coverages. The calculations for the 5 nm particle show that the surface behavior defines the magnetic behavior of the system (see **Inset Fig. 4**). This is expected since the surface spins dominate over the core (71% of the spins are lying on the surface). Consequently, the decrease of the surface anisotropy with the increase of the number of OA molecules is responsible for the observed decrease of the coercive field of the nanoparticle.

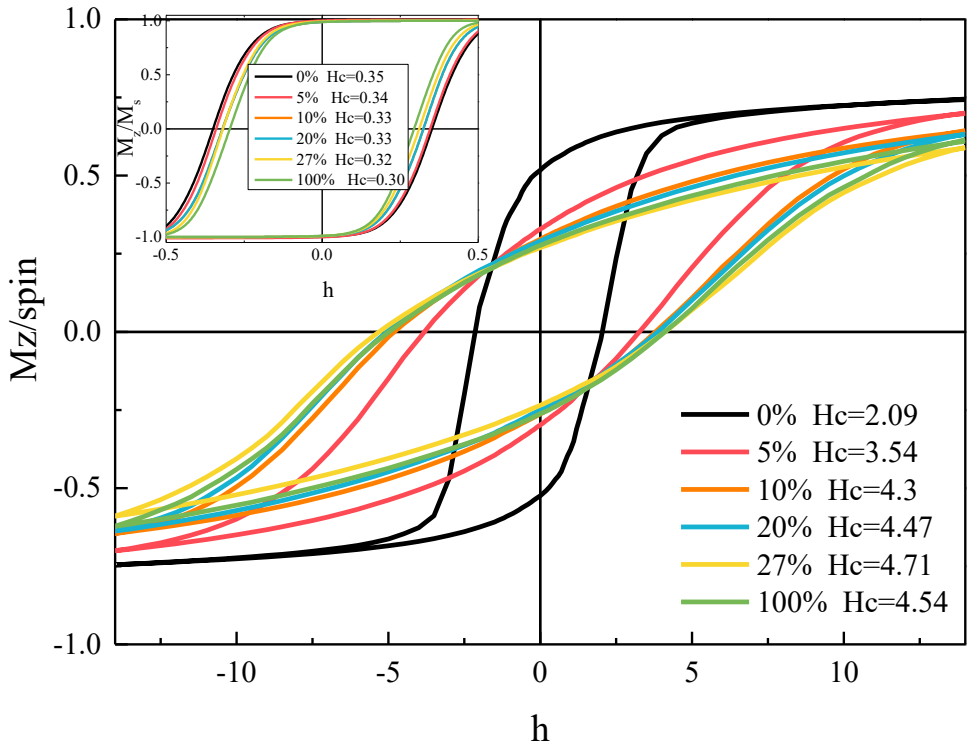

Fig. 4. Monte Carlo simulation results of the hysteresis loops of an assembly of $CoFe_2O_4$ nanoparticles with increasing number of organic molecules attached on their surface, after a field cooling procedure. Inset: The corresponding hysteresis loops of 5 nm Co ferrite nanoparticle. The coercive field Hc is also denoted for each case.

The results for the hysteresis loops of an assembly of nanoparticles for various percentages of OA surface coverage up to the full coverage (100% coating) show an increase of the coercive field with increased OA coverage (**Fig. 4**). This behavior is attributed to the decrease of the exchange coupling (decrease of touching) as the OA coverage at the surface of the nanoparticles increases. However, as coverage increases, the surface anisotropy of each nanoparticle in the assembly decreases and the role of the dipolar interparticle interactions becomes dominant. The dipolar interactions give an extra anisotropy in the assembly and result in the increase of the coercive field [24]. This behavior is in agreement with previous experimental findings [51] for exchange coupled dense assemblies of $CoFe_2O_4$ nanoparticles (~10 nm) in which the coercive field increases with increasing OA surface coverage from 20% to 80%. For the full coverage, the dipolar contribution becomes dominant and at the same time the anisotropy decreases by 20% (see **Table 2**) and the coercive field decreases. This behavior is in agreement with the experimental findings of a dense assembly of $CoFe_2O_4$ nanoparticles (~6 nm) in which the coercive field decreased as the OA surface coverage increased from 80% to 100% [50].

4. Conclusions

We study numerically, for the first time, using a multiscale modeling approach, the effect of OA surface coverage on the magnetic behavior of $CoFe_2O_4$ nanoparticles. Our model with the implementation of DFT calculations on uncoated $CoFe_2O_4$ nanoparticles reveals the surface effects induced by the strong lattice distortion of the surface metal ions. The introduction of the OA molecules bonding on the nanoparticle surface reduces this distortion and as the bonding increases, with the increase of the OA coverage, the coordination symmetry of the bulk material is gradually recovered. Furthermore, we perform Monte Carlo simulations in an atomic scale to investigate this

structural effect on the hysteresis behavior of a larger nanoparticle of 5 nm explicitly including nanoparticle core/surface morphology. The atomic-scale calculations of single $CoFe_2O_4$ nanoparticles further confirm that the increase in OA surface coverage recovers the bulk behavior, resulting in a decrease in the coercive field. Interestingly, our mesoscopic-scale modeling for an assembly of $CoFe_2O_4$ nanoparticles shows that the gradual increase of the OA surface coverage, that gradually reduces the exchange interparticle energy, results in an increase of the coercive field; only in the case of the full OA coverage, where exchange interparticle interactions are not present, is H_C reduced. Our results are in good agreement with available experimental data, paving the way for an optimization of the magnetic behavior of organic-coated MNPs for their use in energy, industrial and biomedical applications.

Corresponding Author

*K.N. Trohidou – Institute of Nanoscience and Nanotechnology, NCSRD, 15310 Agia Paraskevi, Attiki, Greece; http://orcid.org/0000-0002-6921-5419; Email: k.trohidou@inn.demokritos.gr

Author Contributions

The manuscript was written through contributions of all authors. All authors have given approval to the final version of the manuscript. All authors contributed equally.

Declaration of Competing Interest

The authors declare no competing financial interest.

Acknowledgments

The work was supported by the Horizon Europe EIC Pathfinder Programme: under grant agreement No. 101046909 REusable MAsk Patterning (REMAP) https://re-map.eu. Computational time was granted from the Greek Research & Technology Network (GRNET) in the National HPC facility ARIS (http://hpc.grnet.gr) under projects BALCONY (pr 10005) and MNFunction (pr011029).

References

[1] I. Sharifi, H. Shokrollahi, S. Amiri, Ferrite-based magnetic nanofluids used in hyperthermia applications, J. Magn. Magn. Mater. 324 (2012) 903–915. https://doi.org/10.1016/j.jmmm.2011.10.017.

[2] S.Y. Srinivasan, K.M. Paknikar, D. Bodas, V. Gajbhiye, Applications of cobalt ferrite nanoparticles in biomedical nanotechnology, Nanomedicine 13 (2018) 1221–1238. https://doi.org/10.2217/nnm-2017-0379.

[3] S. Behrens, I. Appel, Magnetic nanocomposites, Curr. Opin. Biotechnol. 39 (2016) 89–96. https://doi.org/10.1016/j.copbio.2016.02.005.

[4] M.W. Mushtaq, F. Kanwal, M. Imran, N. Ameen, M. Batool, A. Batool, S. Bashir, S.M. Abbas, A. Ur Rehman, S. Riaz, S. Naseem, Z. Ullah, Synthesis of surfactant-coated cobalt ferrite nanoparticles for adsorptive removal of acid blue 45 dye, Mater. Res. Express. 5 (2018) 035058. https://doi.org/10.1088/2053-1591/aab6a4.

[5] T.T. Nguyen, S. Lau-truong, F. Mammeri, Star-shaped $Fe_{3-x}O_4$-Au core-shell nanoparticles : from synthesis to SERS application, Nanomaterials 10 (2020) 294.

https://doi.org/10.3390/nano10020294.

[6] M. Vasilakaki, I. Chikina, V.B. Shikin, N. Ntallis, D. Peddis, A.A. Varlamov, K.N. Trohidou, Towards high-performance electrochemical thermal energy harvester based on ferrofluids, Appl. Mater. Today 19 (2020) 100587. https://doi.org/10.1016/j.apmt.2020.100587.

[7] C. Scherer, A.M.F. Neto, Ferrofluids: properties and applications, Brazilian J. Phys. 35 (2005) 718–727. https://doi.org/10.1590/S0103-97332005000400018.

[8] R. Wang, F. Han, B. Chen, L. Liu, S. Wang, H. Zhang, Y. Han, H. Chen, Liquid nanoparticles: manipulating the nucleation and growth of nanoscale droplets, Angew. Chemie - Int. Ed. 60 (2021) 3047–3054. https://doi.org/10.1002/anie.202012564.

[9] L. Gutiérrez, L. De La Cueva, M. Moros, E. Mazarío, S. De Bernardo, J.M. De La Fuente, M.P. Morales, G. Salas, Aggregation effects on the magnetic properties of iron oxide colloids, Nanotechnology 30 (2019) 112001. https://doi.org/10.1088/1361-6528/aafbff.

[10] M. Vasilakaki, N. Ntallis, N. Yaacoub, G. Muscas, D. Peddis, K.N. Trohidou, Optimising the magnetic performance of Co ferrite nanoparticles: via organic ligand capping, Nanoscale. 10 (2018) 21244–24253. https://doi.org/10.1039/c8nr04566f.

[11] A.E. Berkowitz, J.A. Lahut, I.S. Jacobs, L.M. Levinson, D.W. Forester, Spin pinning at ferrite-organic interfaces, Phys. Rev. Lett. 34 (1975) 594–597. https://doi.org/10.1103/PhysRevLett.34.594.

[12] R. Costo, M.P. Morales, S. Veintemillas-Verdaguer, Improving magnetic properties of

ultrasmall magnetic nanoparticles by biocompatible coatings, J. Appl. Phys. 117 (2015) 1–8. https://doi.org/10.1063/1.4908132.

[13] S. Sathish, S. Balakumar, Influence of physicochemical interactions of capping agent on magnetic properties of magnetite nanoparticles, Mater. Chem. Phys. 173 (2016) 364–371. https://doi.org/10.1016/j.matchemphys.2016.02.024.

[14] J. Salafranca, J. Gazquez, N. Pérez, A. Labarta, S.T. Pantelides, S.J. Pennycook, X. Batlle, M. Varela, Surfactant organic molecules restore magnetism in metal-oxide nanoparticle surfaces, Nano Lett. 12 (2012) 2499–2503. https://doi.org/10.1021/nl300665z.

[15] C.R. Vestal, Z.J. Zhang, Effects of surface coordination chemistry on the magnetic properties of $MnFe_2O_4$ spinel ferrite nanoparticles, J. Am. Chem. Soc. 125 (2003) 9828–9833. https://doi.org/10.1021/ja035474n.

[16] Z. Hu, X. Yang, R. Liu, X. Chen, Y. He, Y. Hsia, The surfactant influence on the surface magnetic properties of Fe_3O_4 microcrystals, Hyperfine Interact. 57 (1990) 1871–1874. https://doi.org/10.1007/BF02405735.

[17] D.P.G. Muscas, N. Yaacoub, Magnetic disorder in nanostructured materials, in: N. Domracheva, M. Caporali, E. Rentschler (Eds.), Advanced Nanomaterials, Novel Magnetic Nanostructures, Elsevier, 2018, pp. 127–158.

[18] M. Vasilakaki, F. Gemenetzi, E. Devlin, D.K. Yi, S.N. Riduan, S.S. Lee, J.Y. Ying, G.C. Papaefthymiou, K.N. Trohidou, Size effects on the magnetic behavior of γ-Fe_2O_3 core/ SiO_2 shell nanoparticle assemblies, J. Magn. Magn. Mater. 522 (2020) 167570. https://doi.org/10.1016/j.jmmm.2020.167570.

[19] L.F. Cótica, I.A. Santos, E.M. Girotto, E.V. Ferri, A.A. Coelho, Surface spin disorder effects in magnetite and poly(thiophene)-coated magnetite nanoparticles, J. Appl. Phys. 108 (2010) 064325. https://doi.org/10.1063/1.3488634.

[20] J. Lee, Y.H. Choa, J. Kim, K.H. Kim, Comparison of the magnetic properties for the surface-modified magnetite nanoparticles, IEEE Trans. Magn. 47 (2011) 2874–2877. https://doi.org/10.1109/TMAG.2011.2145414.

[21] Y. Köseoğlu, Effect of surfactant coating on magnetic properties of Fe_3O_4 nanoparticles: ESR study, J. Magn. Magn. Mater. 300 (2006) 327–330. https://doi.org/10.1016/ j.jmmm.2005.10.112.

[22] R. Regmi, C. Black, C. Sudakar, P.H. Keyes, R. Naik, G. Lawes, P. Vaishnava, C. Rablau, D. Kahn, M. Lavoie, V.K. Garg, A.C. Oliveira, Effects of fatty acid surfactants on the magnetic and magnetohydrodynamic properties of ferrofluids, J. Appl. Phys. 106 (2009) 113902. https://doi.org/10.1063/1.3259382.

[23] A. Kostopoulou, K. Brintakis, A. Lascialfari, M. Angelakeris, M. Vasilakaki, K. Trohidou, A.P. Douvalis, S. Psycharakis, A. Ranella, L. Manna, A. Lappas, Iron-oxide colloidal nanoclusters: From fundamental physical properties to diagnosis and therapy, in: Prog. Biomed. Opt. Imaging - Proc. SPIE, 2014. https://doi.org/10.1117/12.2039264.

[24] M. Vasilakaki, G. Margaris, D. Peddis, R. Mathieu, N. Yaacoub, D. Fiorani, K. Trohidou, Monte Carlo study of the superspin glass behavior of interacting ultrasmall ferrimagnetic nanoparticles, Phys. Rev. B 97 (2018) 094413(6). https://doi.org/10.1103/ PhysRevB.97.094413.

[25] M. Vasilakaki, N. Ntallis, M. Bellusci, F. Varsano, R. Mathieu, D. Fiorani, D. Peddis, K.N. Trohidou, Effect of albumin mediated clustering on the magnetic behavior of $MnFe_2O_4$ nanoparticles: experimental and theoretical modeling study, Nanotechnology 31 (2020) 025707. https://doi.org/10.1088/1361-6528/ab4764.

[26] K.J.M. Bishop, C.E. Wilmer, S. Soh, B.A. Grzybowski, Nanoscale forces and their uses in self-assembly, Small 5 (2009) 1600–1630. https://doi.org/10.1002/smll.200900358.

[27] T.I. Shabatina, O.I. Vernaya, V.P. Shabatin, M.Y. Melnikov, Magnetic nanoparticles for biomedical purposes: modern trends and prospects, Magnetochemistry 6 (2020) 1–18. https://doi.org/10.3390/magnetochemistry6030030.

[28] D.M.A. Neto, L.S. da Costa, F.L. de Menezes, L.M.U.D. Fechine, R.M. Freire, J.C. Denardin, M. Bañobre-López, I.F. Vasconcelos, T.S. Ribeiro, L.K.A.M. Leal, J.A.C. de Sousa, J. Gallo, P.B.A. Fechine, A novel amino phosphonate-coated magnetic nanoparticle as MRI contrast agent, Appl. Surf. Sci. 543 (2021) 148824. https://doi.org/10.1016/j.apsusc.2020.148824.

[29] B. Bittova, J. Poltierova-Vejpravova, A.G. Roca, M.P. Morales, V. Tyrpekl, Effects of coating on magnetic properties in iron oxide nanoparticles, J. Phys. Conf. Ser. 200 (2010) 072012. https://doi.org/10.1088/1742-6596/200/7/072012.

[30] P. Biehl, M. von der Lühe, S. Dutz, F.H. Schacher, Synthesis, characterization, and applications of magnetic nanoparticles featuring polyzwitterionic coatings, Polymers (Basel) 10 (2018) 91. https://doi.org/10.3390/polym10010091.

[31] G. Baldi, D. Bonacchi, M.C. Franchini, D. Gentili, G. Lorenzi, A. Ricci, C. Ravagli,

Synthesis and coating of cobalt ferrite nanoparticles: A first step toward the obtainment of new magnetic nanocarriers, Langmuir 23 (2007) 4026–4028. https://doi.org/10.1021/la063255k.

[32] Y. Hu, S. Mignani, J.P. Majoral, M. Shen, X. Shi, Construction of iron oxide nanoparticle-based hybrid platforms for tumor imaging and therapy, Chem. Soc. Rev. 47 (2018) 1874–1900. https://doi.org/10.1039/c7cs00657h.

[33] M. Muñoz de Escalona, E. Sáez-Fernández, J.C. Prados, C. Melguizo, J.L. Arias, Magnetic solid lipid nanoparticles in hyperthermia against colon cancer, Int. J. Pharm. 504 (2016) 11–19. https://doi.org/10.1016/j.ijpharm.2016.03.005.

[34] L.S. Arias, J.P. Pessan, A.P.M. Vieira, T.M.T. De Lima, A.C.B. Delbem, D.R. Monteiro, Iron oxide nanoparticles for biomedical applications: a perspective on synthesis, drugs, antimicrobial activity, and toxicity, Antibiotics 7 (2018) 46. https://doi.org/10.3390/antibiotics7020046.

[35] A. Heuer-Jungemann, N. Feliu, I. Bakaimi, M. Hamaly, A. Alkilany, I. Chakraborty, A. Masood, M.F. Casula, A. Kostopoulou, E. Oh, K. Susumu, M.H. Stewart, I.L. Medintz, E. Stratakis, W.J. Parak, A.G. Kanaras, The role of ligands in the chemical synthesis and applications of inorganic nanoparticles, Chem. Rev. 119 (2019) 4819–4880. https://doi.org/10.1021/acs.chemrev.8b00733.

[36] M. Abdolrahimi, M. Vasilakaki, S. Slimani, N. Ntallis, G. Varvaro, S. Laureti, C. Meneghini, K.N. Trohidou, D. Fiorani, D. Peddis, Magnetism of nanoparticles: effect of the organic coating, Nanomaterials. 11 (2021) 1787. https://doi.org/10.3390/nano11071787.

[37] O. Mounkachi, L. Fkhar, R. Lamouri, E. Salmani, A. El, M. Hamedoun, Magnetic properties and magnetoresistance effect of $SnFe_2O_4$ spinel nanoparticles: experimental, ab initio and Monte Carlo simulation, Ceram. Int. 47 (2021) 31886–31893. https://doi.org/10.1016/j.ceramint.2021.08.074.

[38] I.P. Duru, Electronic and magnetic properties of $CoFe_2O_4$ nanostructures: an ab-initio and Monte Carlo study, Phys. B Phys. Condens. Matter. 627 (2022) 413548. https://doi.org/10.1016/j.physb.2021.413548.

[39] H. Liu, C. Di Valentin, Shaping magnetite nanoparticles from first principles, Phys. Rev. Lett. 123 (2019) 186101. https://doi.org/10.1103/PhysRevLett.123.186101.

[40] B. Farkaš, N.H. De Leeuw, Effect of coverage on the magnetic properties of -COOH, -SH, and $-NH_2$ ligand-protected cobalt nanoparticles, Nanoscale 13 (2021) 11844–11855. https://doi.org/10.1039/d1nr01081f.

[41] C. Jo, J. Il Lee, Spin polarization and charge transfer of Co nanoclusters coated with CO molecules, J. Magn. Magn. Mater. 321 (2009) 47–51. https://doi.org/10.1016/j.jmmm.2008.07.036.

[42] M.K. Surendra, R. Dutta, M.S. Ramachandra Rao, Realization of highest specific absorption rate near superparamagnetic limit of $CoFe_2O_4$ colloids for magnetic hyperthermia applications, Mater. Res. Express 1 (2014) 026107. https://doi.org/10.1088/2053-1591/1/2/026107.

[43] M. Kazemi, M. Ghobadi, A. Mirzaie, Cobalt ferrite nanoparticles ($CoFe_2O_4$ MNPs) as catalyst and support: magnetically recoverable nanocatalysts in organic synthesis,

Nanotechnol. Rev. 7 (2018) 43–68. https://doi.org/10.1515/ntrev-2017-0138.

[44] S. Mourdikoudis, A. Kostopoulou, A.P. Lagrow, Magnetic nanoparticle composites: synergistic effects and applications, Adv. Sci. 8 (2021) 2004951. https://doi.org/10.1002/advs.202004951.

[45] T. Dippong, E.A. Levei, Recent advances in synthesis and applications of MFe_2O_4 (M = Co, Cu, Mn, Ni, Zn) nanoparticles, Nanomaterials 11 (2021) 1560. https://doi.org/10.3390/nano11061560.

[46] H. Verma, T. Mekuria, P. Seck, H. Hong, S.P. Karna, D. Seifu, Proximity effect tuned magnetic properties in composites of carbon nanotubes and nanoparticles of $CoFe_2O_4$, J. Magn. Magn. Mater. 501 (2020) 166438. https://doi.org/10.1016/j.jmmm.2020.166438.

[47] P.H. Nam, L.T. Lu, P.H. Linh, D.H. Manh, L.T. Thanh Tam, N.X. Phuc, P.T. Phong, I.J. Lee, Polymer-coated cobalt ferrite nanoparticles: synthesis, characterization, and toxicity for hyperthermia applications, New J. Chem. 42 (2018) 14530–14541. https://doi.org/10.1039/c8nj01701h.

[48] P.B. Kharat, S.B. Somvanshi, P.P. Khirade, K.M. Jadhav, Induction heating analysis of surface-functionalized nanoscale $CoFe_2O_4$ for magnetic fluid hyperthermia toward noninvasive cancer treatment, ACS Omega 5 (2020) 23378–23384. https://doi.org/10.1021/acsomega.0c03332.

[49] Z. Mahhouti, H. El Moussaoui, T. Mahfoud, M. Hamedoun, M. El Marssi, A. Lahmar, A. El Kenz, A. Benyoussef, Chemical synthesis and magnetic properties of monodisperse cobalt ferrite nanoparticles, J. Mater. Sci. Mater. Electron. 30 (2019) 14913–14922.

https://doi.org/10.1007/s10854-019-01863-3.

[50] S. Jovanovic, M. Spreitzer, M. Tramsek, Z. Trontelj, D. Suvorov, Effect of oleic acid concentration on the physicochemical properties of cobalt ferrite nanoparticles, J. Phys. Chem. C 118 (2014) 13844–13856. https://doi.org/10.1021/jp500578f.

[51] M.V. Limaye, S.B. Singh, S.K. Date, D. Kothari, V.R. Reddy, A. Gupta, V. Sathe, R.J. Choudhary, S.K. Kulkarni, High coercivity of oleic acid capped $CoFe_2O_4$ nanoparticles at room temperature, J. Phys. Chem. B 113 (2009) 9070–9076. https://doi.org/10.1021/jp810975v.

[52] R. Lamouri, O. Mounkachi, E. Salmani, M. Hamedoun, A. Benyoussef, H. Ez-zahraouy, Size effect on the magnetic properties of $CoFe_2O_4$ nanoparticles: a Monte Carlo study, Ceram. Int. 46 (2020) 8092–8096. https://doi.org/10.1016/j.ceramint.2019.12.035.

[53] A. Eddahri, S. Razouk, M. Karimou, M.S.M. Sahlaoui, Magnetic behaviors of spinel ferrite nanoparticles: a Monte Carlo simulation, Appl. Phys. A 125 (2019) 1–8. https://doi.org/10.1007/s00339-019-2995-9.

[54] J. Mazo-Zuluaga, J. Restrepo, F. Muñoz, Surface anisotropy, hysteretic, and magnetic properties of magnetite nanoparticles: a simulation study, J. Appl. Phys. 105 (2009) 123907. https://doi.org/10.1063/1.3148865.

[55] G. Kresse, J. Furthmüller, Efficient iterative schemes for ab initio total-energy calculations using a plane-wave basis set, Phys. Rev. B 54 (1996) 11169–11186. https://doi.org/10.1103/PhysRevB.54.11169.

[56] G. Kresse, J. Furthmüller, Efficiency of ab-initio total energy calculations for metals and semiconductors using a plane-wave basis set, Comput. Mater. Sci. 6 (1996) 15–50. https://doi.org/10.1016/0927-0256(96)00008-0.

[57] S.L. Dudarev, G.A. Botton, S.Y. Savrasov, C.J. Humphreys, A.P. Sutton, Electron-energy-loss spectra and the structural stability of nickel oxide, Phys. Rev. B 57 (1998) 1505–1509. https://doi.org/10.1103/PhysRevB.57.1505.

[58] H.J. Monkhorst, J.D. Pack, Special points for Brillonin-zone integrations, Phys. Rev. B 13 (1976) 5188–5192. https://doi.org/10.1039/c8ta11250a.

[59] M. Pénicaud, B. Siberchicot, C.B. Sommers, J. Kübler, Calculated electronic band structure and magnetic moments of ferrites, J. Magn. Magn. Mater. 103 (1992) 212–220. https://doi.org/10.1016/0304-8853(92)90255-M.

[60] C.M. Srivastava, G. Srinivassan, N.G. Nanadifar, Exchange constants in spinel ferrites, Phys. Rev. B 19 (1979) 499–507. https://doi.org/10.1103/PhysRevB.19.499.

[61] N. Daffé, F. Choueikani, S. Neveu, M.A. Arrio, A. Juhin, P. Ohresser, V. Dupuis, P. Sainctavit, Magnetic anisotropies and cationic distribution in $CoFe_2O_4$ nanoparticles prepared by co-precipitation route: Influence of particle size and stoichiometry, J. Magn. Magn. Mater. 460 (2018) 243–252. https://doi.org/10.1016/j.jmmm.2018.03.041.

[62] D. Peddis, F. Orru, A. Ardu, C. Cannas, A. Musinu, G. Piccaluga, Interparticle interactions and magnetic anisotropy in cobalt ferrite nanoparticles: influence of molecular coating, Chem. Mater. 24 (2012) 1062–1071.

[63] C. Vázquez-Vázquez, M.A. López-Quintela, M.C. Buján-Núñez, J. Rivas, Finite size and surface effects on the magnetic properties of cobalt ferrite nanoparticles, J. Nanoparticle Res. 13 (2011) 1663–1676. https://doi.org/10.1007/s11051-010-9920-7.

[64] D. Peddis, N. Yaacoub, M. Ferretti, A. Martinelli, G. Piccaluga, A. Musinu, C. Cannas, G. Navarra, J.M. Greneche, D. Fiorani, Cationic distribution and spin canting in $CoFe_2O_4$ nanoparticles., J. Phys. Condens. Matter 23 (2011) 426004. https://doi.org/10.1088/0953-8984/23/42/426004.

[65] B.D. Cullity, C.D. Graham, Introduction to Magnetic Materials, John Wiley & Sons, Inc., New Jersey, 2008. https://doi.org/http://dx.doi.org/10.1002/9780470386323.fmatter.

[66] E.H. Sánchez, M. Vasilakaki, S.S. Lee, P.S. Normile, G. Muscas, M. Murgia, M.S. Andersson, G. Singh, R. Mathieu, P. Nordblad, P.C. Ricci, D. Peddis, K.N. Trohidou, J. Nogués, J.A. De Toro, Simultaneous individual and dipolar collective properties in binary assemblies of magnetic nanoparticles, Chem. Mater. 32 (2020) 969–981. https://doi.org/10.1021/acs.chemmater.9b03268.

[67] A. Kostopoulou, K. Brintakis, M. Vasilakaki, K.N. Trohidou, A.P. Douvalis, A. Lascialfari, L. Manna, A. Lappas, Assembly-mediated interplay of dipolar interactions and surface spin disorder in colloidal, Nanoscale 6 (2014) 3764–3776. https://doi.org/10.1039/c3nr06103e.

[68] M. Vasilakaki, N. Ntallis, K.N. Trohidou, Application of multiscale computational techniques to the study of magnetic nanoparticle systems, in: Wyrzykowski, R., Deelman, E., Dongarra, J., Karczewski, K. (eds), Parallel Processing and Applied Mathematics. PPAM 2019. Lecture Notes in Computer Science, vol 12044, Springer International

Publishing, 2020: pp. 301–311. https://doi.org/10.1007/978-3-030-43222-5_26.

[69] G. Margaris, K.N. Trohidou, J. Nogués, Mesoscopic model for the simulation of large arrays of bi-magnetic core/shell nanoparticles, Adv. Mater. 24 (2012) 4331–4336. https://doi.org/10.1002/adma.201200615.

[70] A. Walsh, S.H. Wei, Y. Yan, M.M. Al-Jassim, J.A. Turner, M. Woodhouse, B.A. Parkinson, Structural, magnetic, and electronic properties of the Co-Fe-Al oxide spinel system: Density-functional theory calculations, Phys. Rev. B - Condens. Matter Mater. Phys. 76 (2007) 1–9. https://doi.org/10.1103/PhysRevB.76.165119.

[71] M. Vasilakaki, K.N. Trohidou, Surface effects on the magnetic behaviour of nanoparticles with core/shell morphology, J. Phys. D. Appl. Phys. 41 (2008) 134006. https://doi.org/10.1088/0022-3727/41/13/134006.